

Modeling of Mode I Crack Propagation in Fiber Reinforced Concrete by Fracture Mechanics

Jun Zhang and Victor C Li

*Advanced Civil Engineering Materials Research Laboratory
Department of Civil and Environmental Engineering
University of Michigan, Ann Arbor, MI48109-2125, U.S.A.*

ABSTRACT. Mode I crack propagation in fiber reinforced concrete is simulated by a fracture mechanics approach. A superposition method is applied to calculate the crack tip stress intensity factor. The model relies on the fracture toughness of hardened cement paste (K_{Ic}) and the crack bridging law, so called stress-crack width (σ - δ) relationship of the material as the fundamental material parameters for model input. As two examples, experimental data from steel fiber reinforced concrete beams under three point bending load are analyzed with the present fracture mechanics model. A good agreement has been found between model predictions and experimental results in terms of flexural stress versus crack mouth opening displacement (CMOD) diagrams. These analyses and comparisons confirm that the structural performance of concrete and FRC elements, such as beams in bending, can be predicted by the simple fracture mechanics model as long as the related material properties, K_{Ic} and (σ - δ) relationship are known.

KEY WORDS: Mode I Crack Propagation, Crack Bridging, Fiber Reinforced Concrete, Flexural

1. Introduction

The field of fracture mechanics originated in the 1920's with A. A. Griffith's work on fracture of brittle materials such as glass [GRI 21]. Its most significant applications, however, have been for controlling brittle fracture and fatigue failure on metallic structures such as pressure vessels, airplanes, ships etc. Considerable development has taken place in the last thirty years to account for the ductility typical of metals.

Portland cement concrete is a relatively brittle material. As a result, mechanical behavior of concrete, and fiber reinforced concrete is critically influenced by crack propagation. Many attempts have been made to apply the fracture mechanics concept to cement-based composites, such as mortar, concrete and fiber reinforced concrete (FRC). Unlike metallic materials, cement-based materials do not exhibit significant plastic deformations. It seems that linear elastic fracture mechanics might be readily applicable. However, it has been recognized that because of the heterogeneity inherent in the microstructure of concrete, strain softening, microcracking and larger scale process zone, in the order of meter, the fracture parameters such as fracture toughness (K_{Ic}) and fracture energy (G_f) determined in accordance with linear elastic fracture mechanics (LEFM) are size dependent [KAP 61, STR 79]. A relative large microcracking zone called the fracture process zone, where the material behaves nonlinearly, exists adjacent to the crack front, while linear fracture mechanics requires this zone to be small. Therefore, linear elastic fracture mechanics is only applicable to large-scale initially cracked structures and ultrabrittle concrete in which the effect of the nonlinear process zone can be neglected. In all other cases, i.e., for normal-sized concrete structures, especially in fiber reinforced concrete structures, the influence of process zone has to be taken consideration when using the classic linear elastic concepts of fracture mechanics to predict crack propagation. Various models used to describe the fracture process zone in front of a crack of unreinforced and reinforced concrete have been developed, such as (1) the fictitious crack model (FCM) proposed by Hillerborg et al. [HIL 76] and (2) the crack band theory proposed by Bazant et al. [BAZ 83]. The former approach models the process zone as a geometrically discontinuous crack with characteristics after cracking which can be described by a stress-crack opening relationship, so called crack bridging law. The latter imagines the process zone to exist within a certain finite band width in which the microcracks are uniformly distributed and the performance after cracking can be described by a stress-strain relationship. These models are sometimes referred to as cohesive models, or fracture process models, in the literature. In the present work, FCM will be applied to account for the behavior of the process zone.

In the past, some researchers had attempted to use the classical LEFM and crack bridging law to analyze the crack propagation in materials which exhibit crack bridging, such as fiber reinforced ceramics and fiber reinforced concrete (FRC), see Cox et al. [COX 91] and Li et al. [LI 86]. Since a sharp crack tip is still envisaged at the leading edge of the process zone in concrete, reinforced ceramics, even reinforced metals, it is often considered more realistic to assume the bridging force within the process zone will reduce the net stress intensity factor at the crack tip, but not to zero [COX 89; COX 91; LI 86]. This means the crack propagating criteria of linear elastic fracture mechanics remains applicable to above materials, as long as the contribution of the

process zone to the crack tip stress intensity factor is explicitly incorporated. For FRC, crack bridging is a combined aggregate bridging and fiber bridging effect. For concrete, including FRCs, few direct comparisons between experimental results and model predications based on above theory have been carried out. Direct experimental verification is needed in order to utilize the theory in structural design and material optimization with confidence.

In the present paper, mode I crack propagation in unreinforced FRC structure, such as a beam under flexural load, is simulated by the fracture mechanics approach. In this model, the contribution of the crack bridging force to the crack tip stress intensity factor is incorporated in integral form. This approach is very flexible and allows for bridging models for different kinds of FRC materials with different fiber types, volume concentration and matrix properties. A multi-linear model representing the experimental based stress-crack width relationship is adopted for two types of concrete reinforced with straight and hooked steel fibers respectively. The complete theoretical load-crack mouth opening displacement (CMOD) diagrams are obtained and compared with the flexural test results. The results are discussed and conclusions are drawn at the end of the paper.

2. Problem Formulation

In the present model, the fine and coarse aggregates in mortar or concrete are viewed as bridging elements like fibers in concrete, so that the cement paste serves as a fully brittle matrix in concrete and FRC composites. For reasonable size typical of FRC laboratory specimens and structures, the cement paste toughness can be considered a size-independent material property. By this processing, the condition of mode I crack propagation described in the linear elastic fracture mechanics can still be applied to concrete and FRCs as long as the contribution of the bridging force within the process zone to the crack tip stress intensity is included, i.e:

$$K_{tip} = K_{IC} \quad [1]$$

Where K_{IC} is the fracture toughness of cement paste. Thus, the problem reduces to obtaining the crack tip stress intensity factor of the external force and crack bridging respectively.

As an example, a beam under bending load will be considered. Figure 1 shows a cracked beam section with crack length, a and external flexural moment, M . The bridging stress acting on the crack surface along the cracking section is $\sigma_b(\delta(x))$. Based on the superposition scheme shown in Figure 1, the crack tip stress intensity factor can be obtained by summing the contributions K_a of external load and K_b of the bridging force, i.e.

$$K_{tip} = K_a + K_b \quad [2]$$

$$M_a$$

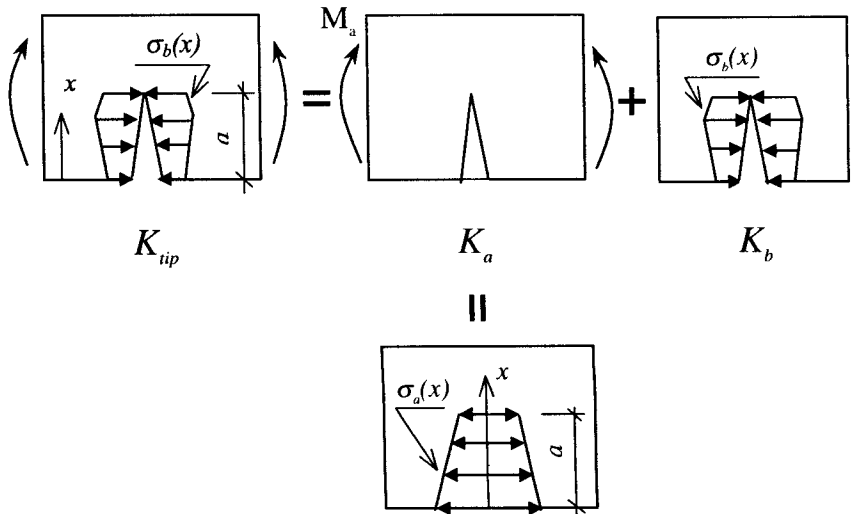


Figure 1. Superposition procedure of solving K_{tip}

The contribution K_a to the stress intensity factor can be calculated through the stress field $\sigma_a(x)$ that would exist on the crack plane in the absence of the crack under specific remote loading, see Figure 1. Under flexural load, $\sigma_a(x) = \sigma_0(0)(1 - 2x/h)$ and $\sigma_0(0) = 6M/bh^2$. Where h and b are depth and width of the beam respectively. Then K_a is calculated by [COX 91]

$$K_a = 2 \int_0^a G(x, a, h) \sigma_a(x) dx \quad [3]$$

Where $G(x, a, h)$ is the weight function that represents the contribution of a unit force on the crack surface to the crack tip stress intensity factor and is specific to body geometry and crack configuration [TAD 85]. For beam under bending, it is given by

$$G(x, a, h) = \frac{h_1(x/a, a/h)}{\sqrt{\pi a (1 - x^2/a^2)^{1/2}}} \quad [4]$$

where

$$h_1(x/a, a/h) = \frac{g(x/a, a/h)}{(1 - a/h)^{3/2}} \quad [5]$$

with $g(x/a, a/h)$ is defined by

$$\begin{aligned}
g(r, s) &= g_1(s) + rg_2(s) + r^2g_3(s) + r^3g_4(s) \\
g_1(s) &= 0.46 + 3.06s + 0.84(1-s)^5 + 0.66s^2(1-s)^2 \\
g_2(s) &= -3.52s^2 \\
g_3(s) &= 6.17 - 28.22s + 34.54s^2 - 14.39s^3 - (1-s)^{3/2} \\
&\quad - 5.88(1-s)^5 - 2.64s^2(1-s)^2 \\
g_4(s) &= -6.63 + 25.16s - 31.04s^2 + 14.41s^3 + 2(1-s)^{3/2} \\
&\quad + 5.04(1-s)^5 + 1.98s^2(1-s)^2
\end{aligned}$$

Similar to the above case, the contribution K_b of the bridging force to the crack tip stress intensity factor can be given by

$$K_b = -2 \int_0^a G(x, a, h) \sigma_b(\delta(x)) dx \quad [6]$$

The fundamental material property of the crack bridging law $\sigma_b(\delta(x))$ will be given as an input. Thus, for a given body geometry, a loading model, a crack configuration, and the crack bridging law, if the crack profile, $\delta(x)$, $x \in (0, a)$ is known, K_{ip} can be calculated by the above equations. And when K_{ip} achieves the K_{IC} value, crack starts to propagate. Now the problem left is how to solving the crack profile for a given crack length. Following the standard derivation outlined in Cox and Marshall [COX 91], the crack opening profile $\delta(x)$ can be related to the applied flexural stress $\sigma_a(x)$ and bridging stress $\sigma_b(\delta(x))$ as

$$\delta(x) = \frac{8}{E} \int_x^a \left\{ \int_0^{a'} G(x', a', h) [\sigma_a(x') - \sigma_b(x')] dx' \right\} G(x, a', h) da' \quad [7]$$

Thus, for a given crack length, a ($a \geq a_0$, a_0 is the initial unbridged flaw size), solving equations [1], [2] and [7] numerically, the critical external load capacity M in terms of flexural stress σ_o and crack profile $\delta(x)$ can be obtained. Then, the conventional flexural strength, so called modulus of rupture (MOR) and load-deformation diagram such as load-crack length and load-CMOD curves which might be more interested to design engineer, can be obtained in above numerical procedure. The detailed numerical scheme can be found in Cox et al. [COX 91].

3. Two Examples - Crack Propagation of Steel FRC Beam under Bending Load

3.1 Experiments

In order to verify the above model, deformation controlled three point bending tests on two types of steel fiber concrete beams, straight fiber and hooked fiber concrete, are carried out. The straight and hooked fibers have circular cross-section, 0.4 mm, 0.5 mm in diameter and 25 mm, 30 mm in length. The beam size is 420x100x100 mm and the bending span is 400 mm. The concrete mixes are listed in Table 1. Here the straight and hooked steel fiber concrete are abbreviated to SSFRC and HSFRC respectively. Some material parameters, such as Young's modulus E and tensile strength σ_t , determined directly from uniaxial tensile test with dog-bone shaped specimen [STA 93] with the same mixes as used for beams, are given in Table 1.

TABLE 1. Mix Propositions of Steel Fiber Concrete

Cement	500 kg/m ³
Sand (maximum particle size 4 mm)	810 kg/m ³
Gravel (maximum particle size 8 mm)	810 kg/m ³
Superplasticizer (66% water content)	3.25 kg/m ³
Water	237.5 kg/m ³
Straight or hooked steel fibers	78.4 kg/m ³

The CMOD is measured by an extensometer with 50 mm gauge length mounted on the middle section of tensile side. Then, CMOD is equal to the measured deformation Δl minus the elastic deformation inside the gauge length. By assuming that stress in the gauge length is equal to the stress transferred by the crack, the CMOD, δ_o is determined from:

$$\delta_o = \frac{\Delta l - \alpha \Delta l_t}{1 + \beta \Delta l_t} \quad [8]$$

where α and β are given by the stress-crack width model shown in Eqn.[9], which reflect the elastic deformation within the gauge length. l is the gauge length and $\Delta l_t = \sigma_t / E$. The experimental setup used for FRC beams in three point bending is shown in Figure 2. The bending test is conducted at a prescribed deformation rate of 0.1 mm per minute using the average signal from the two extensometers used for deflection measurement as feedback. All tests are carried out in a 250-KN capacity, 8500 Instron dynamic testing machine equipped for closed-loop testing.

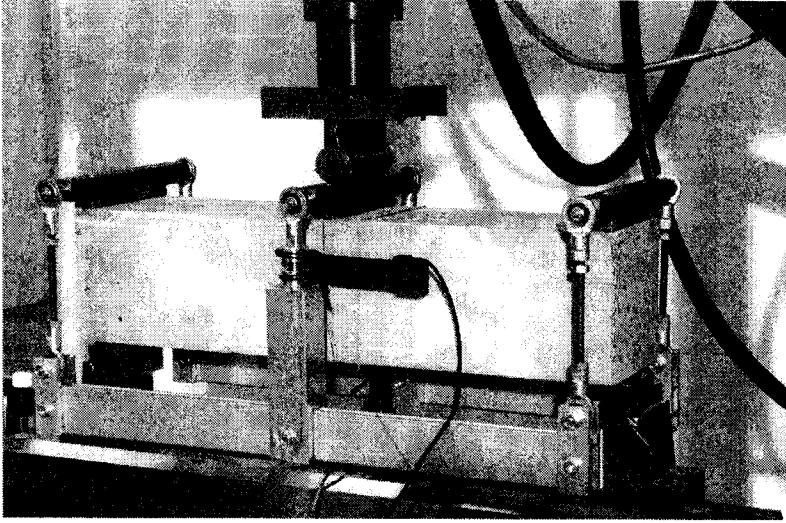


Figure 2. Experimental setup used for FRC beams in three point bending

3.2 Material parameters for model input

The parameters used in the model include fracture toughness of cement paste K_{Ic} , initial unbridged flaw size a_0 and crack bridging law, so called stress crack opening relationship.

(1) Initial unbridged flaw size

According to the model, the initial flaw is an equivalent crack to the initial defects at the tensile face of specimen in the case of bending. These defects might result from air voids, aggregate/cement paste interfacial cracks and other possible damage in the material (e.g. shrinkage cracks). Generally the size of this initial flaw is a function of water/cement ratio, air content and the size distribution of pores in the material. In the present study, a set of initial flaw size a_0 within 0.5 to 4 mm is investigated to find the proper values for unnotched FRC beams. For notched beam, a_0 is equal to the dept of the notch.

(2) Fracture toughness of cement paste

As described in the model, the toughness of cement paste serves as a critical material property in simulating the crack propagation. In the past, few studies had been carried out to determine the fracture toughness of cement paste as well as mortar and concrete [HIG 76; NAU 69; WU 93]. In these studies, the contributions of the process zone is included in calculating the fracture toughness, i.e. the peak load in the load-CMOD curves is used as the critical load for K_{Ic} calculation. Therefore the measured

values of K_{Ic} is strongly influenced by the content of aggregates and is size dependent. However, if the contribution of the process zone is considered in the crack bridging law, then the fracture toughness of cement paste will be a constant, independent of the content of aggregates and is size independent. In both cases, with and without aggregates, the critical load at which crack starts to propagate, i.e. the starting point of the nonlinearity at the load-CMOD curve, should be equal or be quite similar. According to the conventional test method and data processing procedure, the range of the fracture toughness of cement paste is between 0.25 to 0.50 MPa-m^{1/2} (water/cement ratio=0.30–0.50), that is significantly influenced by the water/cement. The K_{Ic} used in present model should be lower than the values mentioned above due to the described reason. For the SFRCs used in the present study (water/cement ratio = 0.475), it is acceptable that K_{Ic} is equal to 0.2 MPa-m^{1/2}.

(3) Crack bridging law

As a fundamental material property, crack bridging laws of cementitious composites, such as mortar, concrete and FRCs had been investigated both experimentally and theoretically during recent years. The experimental results show that the shape of stress-crack width curve of concrete, especially FRC materials is complex and greatly influenced by the type and amount of fiber used [STA 92; AAR 92; ZHA 98]. A micromechanics-based model for stress-crack width relationship of FRC materials has been developed by Li et al. [LI 93] which makes it possible to predict the bridging law of FRC materials with single or hybrid fiber system. The micromechanics-based model provides a basic understanding of the influence of the micro-parameters on the shape of the stress-crack width curve and especially useful for material design. For structural application, a more simplified model is desirable. In this work, a four liner model based on the directly measured stress-crack width (σ - δ) data using both-side notched specimen with the same concrete mixes as used in the beams is used as the crack bridging law, that is

$$\frac{\sigma(\delta)}{\sigma_i} = \alpha_i + \beta_i \delta \quad (i = 1 \dots 4) \quad [9]$$

The coefficients α_i and β_i are listed in Table 2. Because the (σ - δ) model in [9] is based on direct experimental measurements, all contributions of aggregates, fibers as well as hydrated cement particles [HIG 76] to the bridging force in the processing zone are included by it. The comparisons between predictions of the simple model and the experimental data for these two types of FRC are shown in Figure 3. The details of test method for determining stress crack width relationship can be found elsewhere [STA 92; AAR 92; ZHA 98]. Due to the slightly uneven distribution of stress in the cracked section, induced by the notches in the specimen, the measured stress corresponding to a certain crack width is expected to be lower than the real value. Here a (σ - δ) model based on the upper bond of the test data is adopted.

TABLE 2. Material Parameters Used in Four Linear Model for Stress-Crack Width Relationship

Material parameters	SSFRC	δ (mm)	HSFRC	δ (mm)
E(GPa)	35	-	32	-
σ_1 (MPa)	5.42	-	5.30	-
σ_c (MPa)	55.2	-	55.0	-
α_1, β_1 (1/mm)	1, -9.96	0.00-0.03	1, -8.73	0.00-0.04
α_2, β_2 (1/mm)	0.685, 0.526	0.03-0.10	0.632, 0.472	0.04-0.18
α_3, β_3 (1/mm)	0.883, -1.45	0.10-0.38	0.800, -0.463	0.18-0.75
α_4, β_4 (1/mm)	0.374, -0.110	0.38-2.00	0.532, -0.106	0.75-2.00

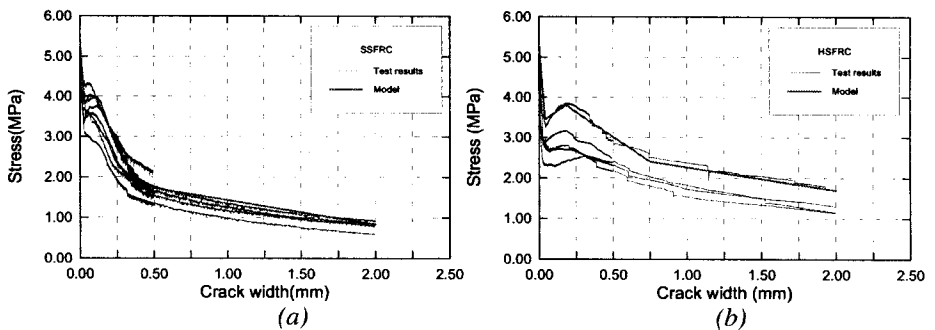


Figure 3. Measured stress-crack width data and four linear model predictions, (a) SSFRC (b) HSFRC

4. Results and Discussion

In this section, the crack propagation of beams made of SSFRC and HSFRC respectively, under bending load is simulated with the current model. The influence of initial flaw size a_0 and the fracture toughness K_{Ic} on the flexural performance of FRC beams are presented and discussed first. Later, model predictions are compared with the experimental results and appropriate parameters of a_0 corresponding to K_{Ic} is proposed. Finally, some discussions on the flexure performance steel fiber concrete are given.

4.1 Effect of initial flaw size and fracture toughness

Figure 4 shows the results of the effect of initial unbridged flaw size on the flexural behavior in terms of flexural stress versus crack length diagrams. From these curves, it can be seen that for a given K_{Ic} , the larger the a_0 , the lower the first crack strength and the flexural strength (MOR). Due to the dependence of the initial flaw size a_0 on various material parameters, the value of a_0 can only be estimated according the experimental results for a given K_{Ic} .

Figure 5 shows the results of the effect of K_{IC} on the flexural behavior in terms of flexural stress versus crack length curves. From this figure, it can be found that the first crack strength is increased with higher cement paste fracture toughness. With the increase of crack length, the behavior is more controlled by the crack bridging, while the influence of K_{IC} is gradually reduced. Even so, the conclusion can be made that the fracture toughness of cement paste can significantly influence the flexural performance of cementitious composite beams. For example, the fracture behavior of the beam under bending load can vary from ductile to brittle with the change of the fracture toughness of the cement paste, as shown in Figure 5. Here it is assumed that the crack bridging stress is not influenced by the fracture toughness of cement paste.

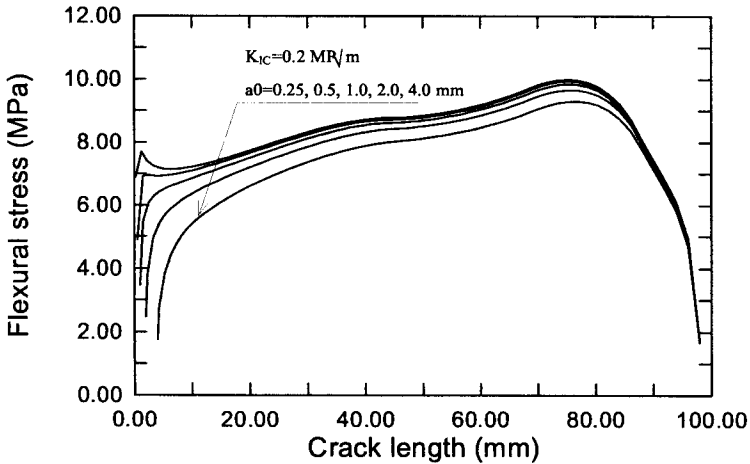


Figure 4. Effect of initial flaw size a_0 on the bending performance, in terms of flexural stress versus crack length curves

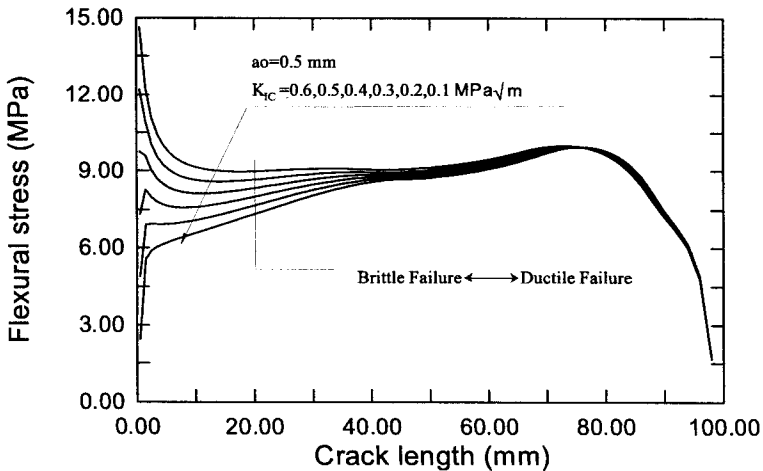


Figure 5. Effect of K_{IC} on the bending performance, in terms of flexural stress versus crack length curves

4.2 Comparison with experimental data and discussions

By comparing the model results with experimental data, for present SFRCs, it is found that with a_p equal to 0.5mm and K_{IC} is equal to 0.2 MPa-m^{1/2}, very good fit can be obtained. The comparisons are given by Figures 6 to 9.

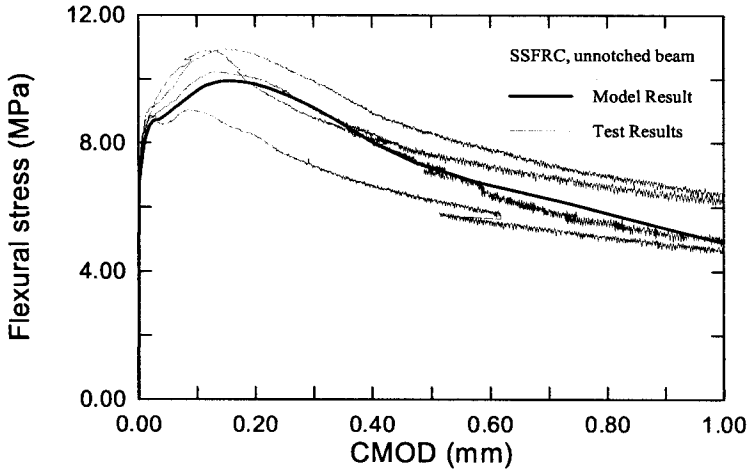


Figure 6 Comparison between model prediction and the experimental results in terms of flexural stress-CMOD curves of SSFRC beams

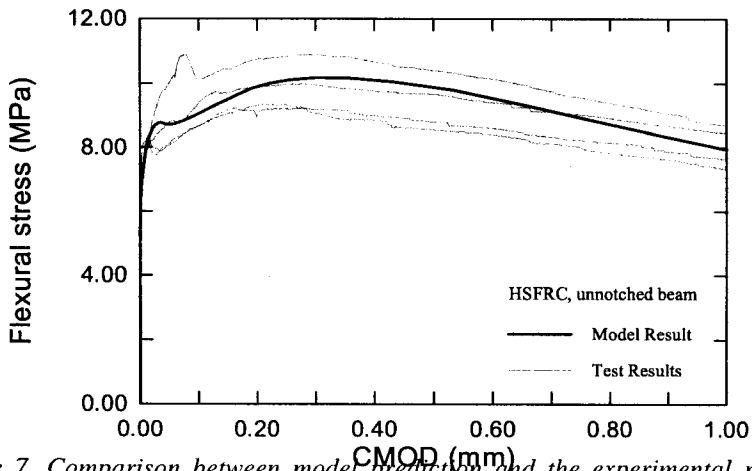


Figure 7. Comparison between model prediction and the experimental results in terms of flexural stress-CMOD curves of HSFRC beams

In Figures 6 and 7 comparisons are shown between model predictions and experimental data in terms of load-CMOD curves in the range of 0 to 1.0 mm for both kinds of steel FRCs. From these figures, first it follows that very good agreement can be

obtained between present model predicted and experimental measured load-CMOD diagrams. Second, the load-deformation curve can be divided into three sections:

- (1) elastic stage up to first crack stress σ_{fc} , which is a function of K_{IC} and a_0 , with a constant stiffness ($d\sigma/d\delta$).
- (2) crack developing stage one, load increases with a slow reduction on the stiffness of beam until the crack length reaches about 40% of the beam depth, see Figures 8 and 9.
- (3) crack developing stage two, load increases with significantly reduced stiffness until peak load at which the stiffness become zero, then load capacity starts to reduce with a negative stiffness.

In stages (1) and (2), the structural performance of SSFRC and HSFRC beams are almost identical, as shown in Figures 8 and 9. The load capacity reaches about 90% of its ultimate load with a limited deformation level, 0.025 mm for CMOD at the end of stage (2). In the stage (3), load increases a little (10% of its ultimate load) with significant increase in deformation. At this point, the difference on load-deformation behavior of SSFRC and HSFRC beams becomes pronounced. HSFRC beam can absorb more energy than SSFRC beam. In other word, the toughness of materials can be increased by hooks. From these results, the CMOD and crack length at peak load of SSFRC and HSFRC beams are 0.15 mm, 0.75h and 0.35 mm, 0.80h respectively. This also indicates that the shape of load-CMOD curves depends strongly on the shape of the stress-crack width curve. This shows us that in order to improve bending performance, the bridging behavior of materials has to be improved first. As a fundamental material property of FRC, the bridging law is of notable significance in optimizing the structural properties of FRC structures, including the static performance such as tension and bending, as well as cyclic performance such as impact and fatigue. It also can be found from the figures that the first crack stress σ_f is much lower than ultimate stress (MOR) in these two FRC beams. This is because a stable process zone grows after cracking which leads to the flexure strength higher than the first crack strength of the materials. The flexure strength is size dependent as unstable growth of the process zone depends on the ligament dimension ahead in the beam. Detailed study of this size-dependency is presented in [LI 98].

5. Conclusions

A fracture mechanics approach for modeling the mode I crack propagation in FRCs and further to obtain the flexure behavior of FRC beams has been presented. The model relies on the stress-crack width relation as the fundamental relationship in calculating the crack tip stress intensity factor (K_{np}) with the superposition method. Very good agreement has been found between model predictions and experimental results in terms of load-CMOD diagrams. The important structural parameters for designer such as bending toughness, ultimate load as well as the corresponding deformation response can easily be obtained through the present model.

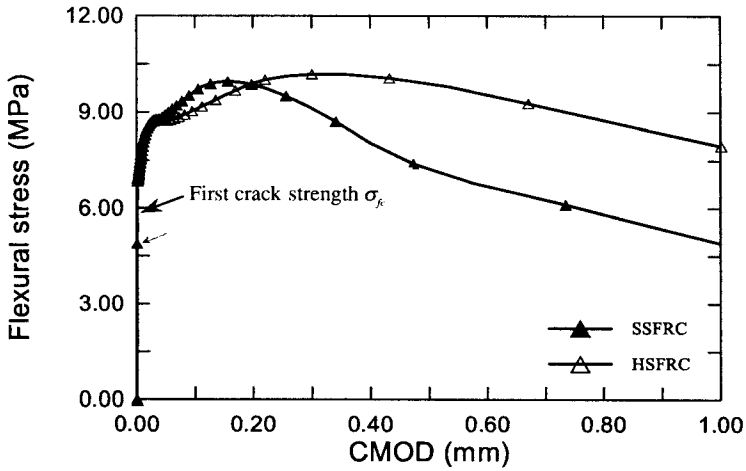


Figure 8. Model predicted flexural stress versus CMOD curve, shown both kinds of FRC beams together

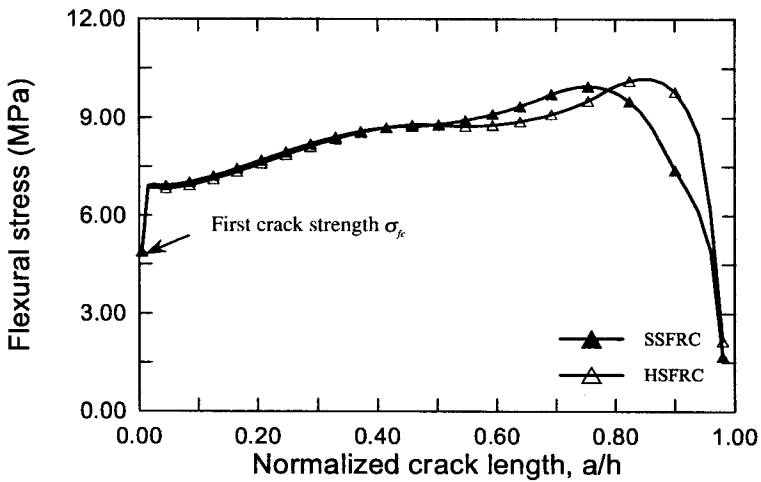


Figure 9. Relationship between flexural stress and crack length of both FRC beam under three point bending, model results

From this model it can be deduced that the flexural performance is strongly dependent on the stress-crack width relation of materials. The optimal bending behavior of FRC structures can be achieved through optimizing the bridging behavior of aggregates and fibers.

This model can be extended to other types of specimens and load configurations, such as uniaxial tension and compact tension.

Acknowledgements

This work has been supported by a grant from the National Science Foundation (CMS-9872357) to the University of Michigan.

6. References

- [AAR 92] Aarre, T., "Tensile characteristics of FRC with special emphasis on its applicability in a continuous pavement", Ph.D thesis, Department of Structural Engineering and Materials, Technical University of Denmark, Serie R, n^o 301, 1992.
- [BAZ 83] Bazant, Z.P., and Oh, B.H., "Crack band theory for fracture of concrete", *Material and Structure*, vol. 16, p.155-177, 1983.
- [COX 89] Cox, B.N. and Marshall, D.B. and Thouless, M.D., *Acta Metall. Mater.*, vol. 37, n^o 7, p. 1933-1943, 1989.
- [COX 91] Cox, B.N. and Marshall, D.B., "Stable and unstable solutions for bridged cracks in various specimens", *Acta Metall. Mater.*, Vol. 39, n^o 4, p. 579-589, 1991.
- [GRI 21] Griffith, A.A., "The phenomena of rupture and flow in solids", *Phil. Trans. Roy.Soc.*, series A221, p.163-168, 1921.
- [HIG 76] Higgins, D.D. and Bailey, J.E., "Fracture measurement on cement paste", *Journal of Materials Science*, vol. 11, p. 1995-2003, 1976.
- [HIL 76] Hillerborg, A., Mod er, M. and Petersson, P-E., "Analysis of crack formation and crack growth by means of fracture mechanics and finite elements", *Cement and Concrete Research*, vol. 6, p.773-782, 1976.
- [KAP 61] Kaplan, F.M., "Crack propagation and fracture of concrete", *Journal of the American of Concrete Institute, Proceedings*, vol. 58, n^o 5, p.591-610, 1961.
- [LI 86] Li, V.C. and Liang, E., "Fracture processes in concrete and fiber reinforced cementitious composites", *Journal of Engineering Mechanics*, vol. 112, n^o 6, p566-586, 1986.
- [LI 93] Li V.C., Stang, H. and Krenchel, H., "Micromechanics of crack bridging in fibre reinforced concrete", *Materials and Structures*, vol. 26, p.486-494, 1993.
- [LI 98] Li, V.C., Lin Z. and Matsumoto, T., "Influence of fiber bridging on structural size-effect", *International Journal of Solid and Structures*, vol. 35, n^o 31-32, p. 4223-4238, 1998.
- [NAU 69] Naus, D.J. and Lott, J.L., "Fracture toughness of portland cement concrete", *Journal of American Concrete Institute*, June, p. 481-489, 1969.
- [STR 79] Strange, P.C. and Bryant, A.H., "Experimental tests on concrete fracture", *ASCE Proc., Journal of the Engineering Mechanics Division*, vol. 105, p.337-342, 1979.
- [STA 92] Stang, H. and Aarre, T., "Evaluation of crack width in FRC with conventional reinforcement", *Cement and Concrete Composites*, vol. 14, n^o 2, p.143-154, 1992.
- [STA 93] Stang, H., *Newpave Report*, Department of Structural Engineering and Materials, Technical University of Denmark, 1993.
- [TAD 85] Tada, H., *The stress analysis of cracks handbook*, Paris Prod. Inc., 1985.
- [WU 93] Wu, H.C., Mishra, D.K. and Li, V.C., Influence of matrix fracture toughness on tensile behavior of fiber reinforced cementitious Composites, in *Proceedings of the Symposium on Cement and Concrete*, Beijing, China, 1993.
- [ZHA 98] Zhang, J., *Fatigue Fracture of Fiber Reinforced Concrete*, Ph.D thesis, Department of Structural Engineering and Materials, Technical University of Denmark, Serie R, n^o 41, 1998.

Figure Captions

Figure 1. Superposition procedure of solving K_{ip}

Figure 2. Experimental setup used for FRC beams in three point bending

Figure 3. Measured stress-crack width data and four linear model predictions, (a) SSFRC (b) HSFRC

Figure 4. Effect of initial flaw size a_0 on the bending performance, in terms of flexural stress versus crack length curves

Figure 5. Effect of K_{Ic} on the bending performance, in terms of flexural stress versus crack length curves

Figure 6 Comparison between model prediction and the experimental results in terms of flexural stress-CMOD curves of SSFRC beams

Figure 7. Comparison between model prediction and the experimental results in terms of flexural stress-CMOD curves of HSFRC beams

Figure 8. Model predicted flexural stress versus CMOD curve, shown both kinds of FRC beams together

Figure 9. Relationship between flexural stress and crack length of both FRC beam under three point bending, model results